J Nanostruct 9(3): 510-520, Summer 2019

RESEARCH PAPER

Investigation of the Effect of Argon Flow on the Morphology of B_4C Nanoparticles Synthesized by the VLS Method

*Ali Alizadeh *, Mohammadreza Mahoodi*

Faculty of materials and manufacturing processes, Malek Ashtar University of Technology, Tehran, Iran

ARTICLE INFO

Article History:
Received 22 January 2019
Accepted 26 April 2019
Published 01 July 2019

Keywords:
Activated Carbon
Argon Gas Flow
Boron Carbide Synthesis
Carbon Black
Nanowires
VLS

ABSTRACT

In this paper, new various morphologies of boron carbide were successfully synthesized using carbon black, activated carbon and boron oxide precursors as well as using cobalt nanoparticles as catalysts. Almost the whole morphology of synthesized boron carbide are consisted of smooth nanowires and nanobelts. With decreasing the carbon black particles size from 29 nm to 13 nm (29, 23, 17 and 13), the synthesis efficiency of nanowires and nanobelts are increased. With increasing the temperature from 1500 °C to 1700 °C, the amounts of nanowires and nanobelts are decreased and the amounts of nano particles and synthesizing the nanoworms are increased. By placing the catalyst nanoparticles on the crucible lid and being subjected to the argon gas flow, new morphologies of boron carbide are appeared (flower-shaped and needle-shaped are synthesized by using carbon black and activated carbon, respectively). The argon gas flow creates new branches on the main wires. The specimens were characterized by the X-ray diffraction and a scanning electron microscopy.

How to cite this article
Alizadeh A, Mahoodi MR. Investigation of the Effect of Argon Flow on the Morphology of B_4C Nanoparticles Synthesized by the VLS Method. J Nanostruct, 2019; 9(3): 510-520. DOI: 10.22052/JNS.2019.03.012

INTRODUCTION

Boron carbide is a crystalline material with the chemical formula of $B_{12}C_3$ and a rhombohedral crystal structure [1]. Its melting point is 2450 °C [2], its density is 2.51 g/cm^3 [2], its fracture toughness (K_{IC}) is around 3.7-2.9 MPa.m$^{1/2}$, its Young modulus is about 460-360 GPa [3], its hardness is 35 GPa and its coefficient of thermal expansion is 5.73 × 10^{-6} K^{-1} [4]. Boron carbide is one of the hardest materials after diamond and cubic boron nitride [5]. This material is a p-type semiconductor with the band gap of 0.8 eV, exhibits high chemical resistance and is a neutron absorber [6]. Owing to its numerous unique properties, B_4C has found many applications such as neutron moderator in nuclear reactors, wear resistant tools and bullet-proof blocks [1–6]. There are different synthesized boron carbide structures including s, nanorods, nanobelts, nanoparticles, etc. [4]. In addition, there are many routes for the synthesis of B_4C such ad plasma-enhanced chemical vapor deposition for nanowires [7–9], electrospinning for nanorods [10], carbothermal reduction reaction for powders, magnesiothermic reduction reaction for powders and vapor-liquid-solid reaction for nanowires and nanobelts [4,11]. Bao Li-Hong et al. synthesized a high amount of B_4C nanowires using $B/B_2O_3/C$ precursors at 1100 °C by the VLS carbothermal reduction [12].

These methods each have some shortcomings as well as advantages. Some methods such as the catalyst unassisted thermal evaporation and PECVD result in high quality nanostructures but in them the yield of products is low and large-scale synthesis may be expensive. Some others such as AAO templating, carbon nanotube template based

* *Corresponding Author Email: alizadehh53@gmail.com*

and electrostatic spinning use rare expensive starting materials. Carbothermal reduction of boron oxide in the presence of catalyst metallic particles is a low-cost method but the products yielded thereof contain a significant amount of remained carbon; the elimination of the excess carbon is not easy.

The above-mentioned methods may be very suitable for some particular applications [5], but when the application of boron carbide nanostructures is intended as a reinforcing phase, purification dispensability and chemical homogeneity of reinforcing particles besides low-cost and facile large-scale synthesis capability become the most important factors. In this case, the excellent quality of nanostructures and morphological homogeneity are depressed to next precedence. Therefore, developing a method with large-scale and low-cost synthesizing capability is still needed.

Regarding the high melting point of boron carbide, the VLS carbothermal method can decrease significantly the temperature required for the synthesis of B_4C. Therefore, according to the studies carried out earlier, the temperature range used can be around 1700 °C [6,12–14]. Despite all the positive aspects, this method suffers from limitations, the most important of which, is the high amount of 2D structures including nanobelts and nanoworms.

This method has problems with all the features. The main problems are: 1) the large volume of two dimensional nanostructures by different morphology synthesizing including nanobelts, nanoworm 2) morphology of the synthesized samples is uncontrollable.

The aim of this research is the synthesis of a reinforcing mixture containing boron carbide nanostructures in a large scale via a facile and low-cost method. The mentioned mixture is expected to have an enhanced reinforcing capability due to elongated shapes of the nanostructures [15,16]. However, in the present method, for kinetic reasons, the starting powder is not completely converted to the mentioned nanostructures and initial B_4C powders are somewhat remained in the final product but this morphological inhomogeneity is not disadvantageous at all [16–18] because the starting powders have also reinforcing effects; besides boron carbide particles are currently used as a reinforcing phase in different composite materials [19–21]. It is

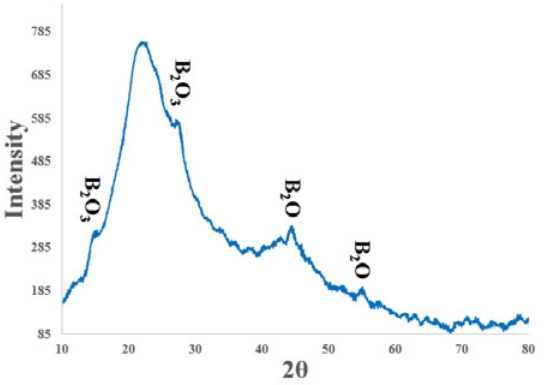

Fig. 1. The XRD pattern of the boron oxide used as the starting material.

well known that elongated nanostructures (such as nanowires, nanorods and nanobelts) have enhanced reinforcing effects due to both nanosize effects and morphological characteristics [15,22,23]. The final product, which contains boron carbide initial powders accompanied by nanowires, nanobelts and nanosheets, might exhibit an improved reinforcing effect due to the presence of elongated nanostructures [16,24–26]. Amorphous carbon as a potent reducing agent is one of the precursors of the synthesis of boron carbide, which is used in both carbon-active and carbon-black forms. With its unique chemical and structural properties, carbon black have completely different effect on nanowires synthesis. Also, Argon gas flow facilitates and accelerates the availability vapors to the catalyst.

This study is aimed at the synthesis of B_4C nanowires by the CVD carbothermal method using the VLS growth mechanism along with Co nanoparticles as the catalyst, activated carbon, carbon black and boron oxide as the precursors. The CVD method was used for the synthesis of a high amount of B_4C nanowires. Moreover, the VLS growth mechanism led to smooth surfaces on the synthesized nanowires at the presence of Co nanoparticles as the catalyst. Amorphous carbon is used as a strong reducing agent and one of the precursors for the synthesis of B_4C which is used in two forms of carbon black and activated carbon. Carbon black can exhibit outstanding effects on the synthesis of nanowires owing to its unique chemical and structural properties. Argon flow accelerates and eases vapor access to the catalyst.

Table 1. The row materials and their characteristics

Raw materials	Production company	Pure (%)	Particle size	Aim of use
B_2O_3	Merck	99	$< 3\mu m$	Boron precursors
NaCl	Merck	99.8	-	Gas reactor
Ethanol	Degussa	99	-	Environment milling
Cobalt	IoliTec	99.99	30nm	catalyst
Carbon Black (B1)	Degussa	79	29nm	Carbon precursors
Carbon Black (B2)	Degussa	79	23nm	Carbon precursors
Carbon Black (B3)	Degussa	79	17nm	Carbon precursors
Carbon Black (B4)	Degussa	79	13nm	Carbon precursors
Carbon Active (A)	Merck	99	$< 10\mu m$	Carbon precursors

MATERIALS AND METHODS

The starting materials are listed in Table 1.

In this research, the VLS carbothermal reduction was used to synthesize B_4C nanowires. An attrition mill was employed to mix the powders. First, the molar ratio of B_2O_3:C:NaCl:Co=2:4:0.25:0.1 was selected to blend the powders [4,11]. B_2O_3, C, NaCl, and Co were mixed according to the above-mentioned molar ratio in an attrition mill containing 1 Kg of steel balls (5 mm diameter) in an ethanol medium for 1 hour. The powder to ball ratio was 1:20 and the ratio of the occupied chamber volume to the total mill volume was 1:4. Then, the Co powder hold in ethanol for 30 min was placed in an ultrasonic bath and then was added to the milled mixture. The entire mixture was ultrasonicated for 30 min. a magnetic heater was used to remove ethanol. The solution underwent filtration for 4 hours to separate coarse particles. the graphite substrate was cleaned by HCl and rinsed with water. One gram of the mixture was poured into a graphite substrate with the dimensions of 25 cm x 25 cm x 25 cm. Then, the crucible was placed in a tube furnace

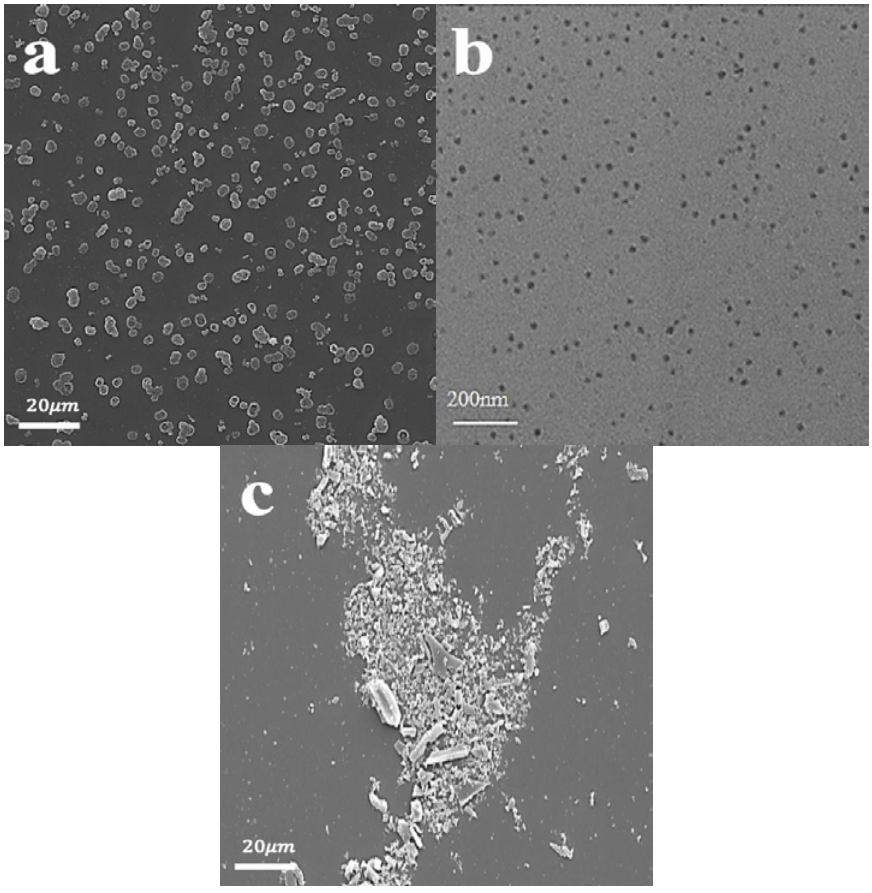

Fig. 2. The SEM image of (a) boron oxide (b) catalyst and (c) activated carbon.

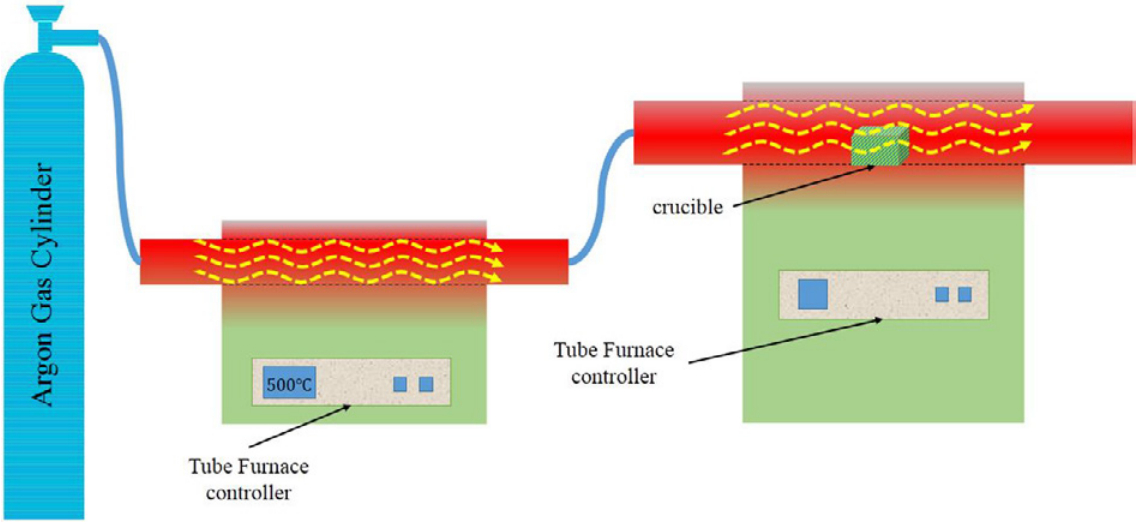

Fig. 3. The schematic of the process used in the test along with its configuration.

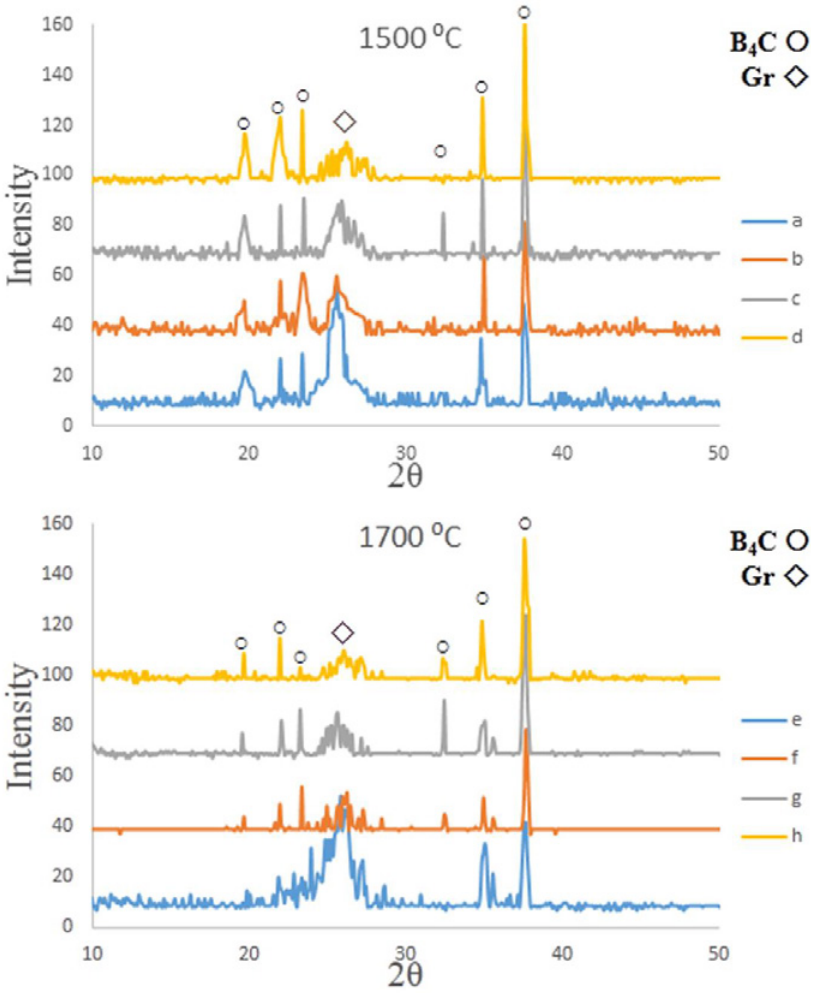

Fig. 4. The XRD patterns of the B_4C synthesized using carbon black at 1500 °C (a) B1 (b)B2 (c) B3 (d) B4. The XRD patterns of the B_4C synthesized using carbon black at 1700 °C (e) B1 (f) B2 (g) B3 (h) B4.

for 90 min under the argon gas flow (700 cm^3/ min) at 1500 °C and 1700 °C. The argon gas was preheated to 500 °C by passing it in another tube furnace. After the optimization of the synthesis parameters, two-dimensional B_4C nanostructures were poured on the crucible lid to study the direct effect of the argon gas flow on the morphology of the two-dimensional B_4C nanostructures.

In order to detect the formed phases as well as performing the morphological investigation on the synthesized samples, X-ray diffraction (XRD- siefert 3003, Cu K_α, Y= 1.5406 A) and a scanning electron microscope (SEM- LEO 1450VP) were used, respectively. Before using the SEM, the samples were coated with gold.

RESULTS AND DISCUSSION

Fig. 4 shows the samples synthesized using carbon black at 1500 °C and 1700 °C. The pattern can be indexed to rhombohedra B_4C crystal (the JCPDS card 35-0798). As can be observed, B_4C peaks are evident in all the samples. In addition, an increasing trend for the B_4C formation and a decreasing trend for the remained carbon with decreasing the carbon particle size are obvious. With decreasing the carbon particle size, the specific area of these particles increases which results in the easier consumption of the particles. At 1700 °C, a positive trend for the formation of B_4C as well as the negative trend of the remained carbon has been continued in the sample with decreasing the carbon particle size. It was expected that with increasing the synthesis temperature from 1500 °C to 1700 °C, a more driving force was provided for the B_4C synthesis formation. However, the amount of the B_4C synthesized at 1700 °C is almost equal to that synthesized at 1500 °C but the decreasing trend for the remained carbon has been continued. Three peaks with lower 2θ are found in the samples synthesized at 1700 °C which are much sharper than those of the samples synthesized at 1500 °C. These sharper peaks are indicative of a product with a higher degree of crystallinity.

Fig. 5 shows the XRD patterns of the samples synthesized at 1500 °C and 1700 °C. Although all the samples equal ratios of the starting materials, a higher amount of B_4C has been synthesized in the sample containing activated carbon.

Fig. 6 shows the SEM images of the samples at 1500 ° C. In B1, no wires are seen. With reducing the carbon particle size, the amount of nanowires are increased. Thus, with the reduction of carbon particle size, the amount of synthesized wire is increased in B1, B2, B3, and B4. It should be noted that with decreasing the particle size, the reactivity of the particles increases while the melting temperatures of the materials decreases [27]. The increase in reactivity contributes to the formation of two-dimensional nanostructures that is resulted from more activation of the VLS growth mechanism this is clearly seen in the figures. Also, it can be seen that nanowires and nanobelts are most of the visible structures in these images. As can be seen in the images of B4 and A samples at 1500 °C, the sample containing activated carbon have a much higher amount of nanoworms compared with the sample containing carbon black.

The SEM images of sample B4 and A at 1700 °C are shown in Fig. 7. As seen in this figure, the amounts of the synthesized nanowires and

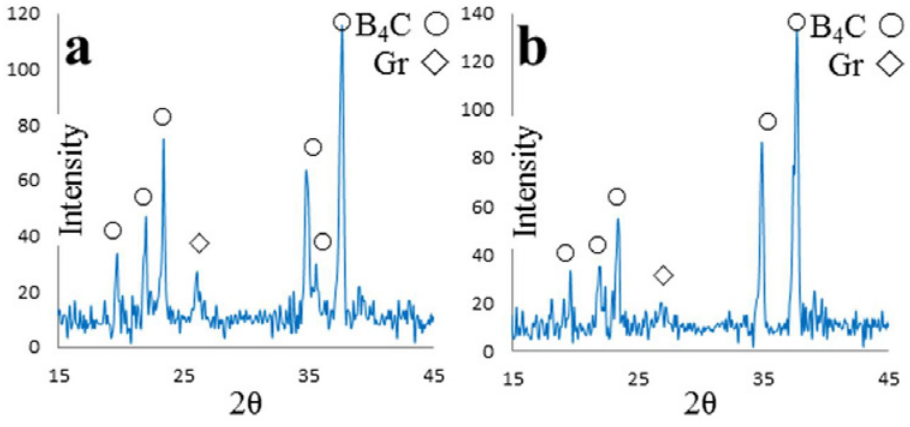

Fig. 5. The XRD patterns of the B_4C synthesized using activated carbon (a) at 1500 °C and (b) at 1700 °C.

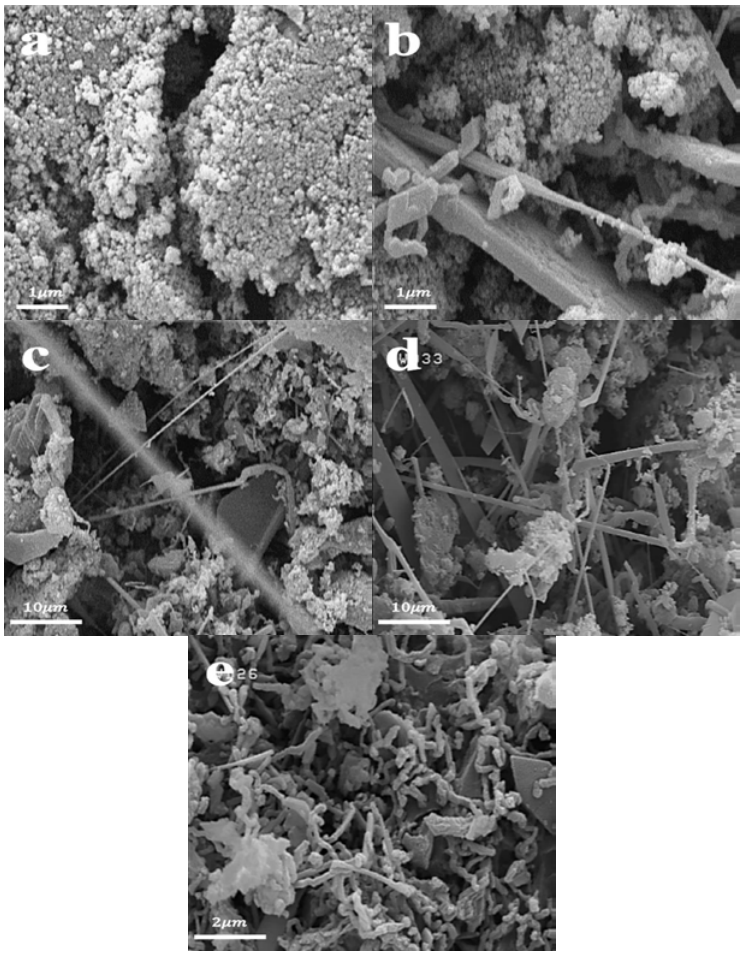

Fig. 6. The SEM image of the amount of the nanowires synthesized at 1500 °C. (a) Sample B1 in which, no nanowire has been synthesized. (b) Sample B2 which contains nanowires and nanobelts. (c and d) Samples B3 and B4, respectively in which, increasing the amounts of nanowires and nanobelts can be observed. (c) The wires, nanobelts and nanoworms synthesized in sample A.

nanobelts have decreased significantly, the trends of which are against B_4C particles. Thus, the synthesized wires are obtained thicker and contain larger particles at this temperature. Before the VLS mechanism to active, the row materials get the need energy to react with each other, and instead of the wires B_4C particles are formed. The sharper pattern of the XRDs of the samples synthesized at 1700 °C can be justified by the decreased amount of nanobelts and nanowires (semi-crystalline) and the increased in the amount of boron carbide particles (fully crystalline) [4].

In this type of synthesis process, both the VLS and SLS mechanisms is activated in which a metallic catalyst is used [27-29]. In the VLS mechanism, in first the melted alloy droplets are created, then the vapors are absorbed by the catalyst droplets in the surrounding area, and after reaching the supersaturation stage the two-dimensional nanostructures growth are begun from the catalyst droplets. On the other hand, the vapors can be reacted directly with each other and be formed the B_4C particles. In the SLS mechanism, the catalyst droplets are combined with B_4C and the droplets containing boron and carbon are formed. Boron and carbon are introduced in the catalyst droplets either by the direct dissolution of B_4C powder available in the B_4C powder/catalyst droplet interface or through the surface penetration of the components. Ultimately, boron and carbon are precipitated in the droplets and formed the crystalline nanostructures [4]. The reactions which occur during the VLS and SLS mechanisms are as follow:

VLS mechanism

$$NaCl_{(L)} \rightarrow NaCl_{(g)} \rightarrow Na_{(g)} + Cl_{(g)} \quad (1)$$

$$B_4C_{(s,Powder)} + Cl_{(g)} \rightarrow 4BCl_{(g)} + C \quad (2)$$

$$Co_{(L)} + C_{(s)} \rightarrow Co - C_{(L)} \quad (3)$$

$$Co - C_{(L)} + 4BCl_{(g)} \rightarrow Co - C - B_{(L)} + CoCl_{2(g)} \quad (4)$$

$$Co - C - B_{(L)} \rightarrow B_4C_{(s,elongated\ nanostructures)} + Co_{(L)} \quad (5)$$

SLS mechanism

$$B_4C_{(s,Powder)} + Co_{(L)} \rightarrow Co - C - B_{(L)} \rightarrow B_4C_{(s,elongated\ nanostructures)} + Co_{(L)} \quad (6)$$

According to the as-mentioned discussion, the temperature directly was determined the formation type and the growth mechanism of B_4C nanostructures. As seen in the images taken from the samples at 1500 °C and 1700 °C, (1500 °C) the VLS and SLS mechanisms were overcame on the B_4C particles formation mechanism at the lower temperatures and the opposite of the above was occurred at higher temperatures (1700 °C). Therefore, samples A and B4 were selected as the samples containing the optimum particle sizes and the temperature of 1500 °C was chosen as the optimal temperature.

Fig. 8a and b shows the SEM image of sample B4 at 1500 °C when the catalyst is applied to the crucible lid. Since owing to argon flow, the catalyst can be moved for a short distance, so the catalyst droplets can be joined each other to make the

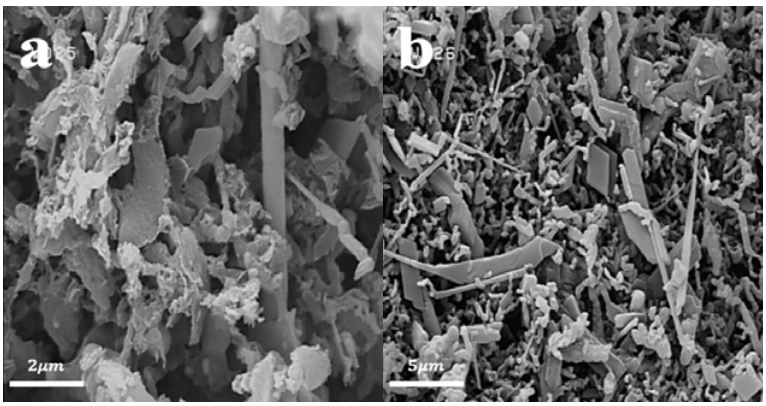

Fig. 7. The SEM image of B4 (a) and A (b) at 1700 °C.

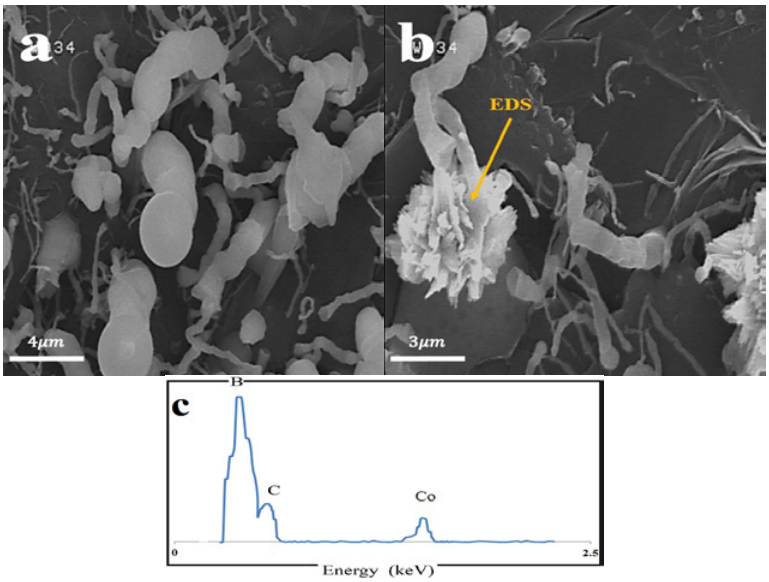

Fig. 8. the SEM image of B4 when the catalyst is applied to the crucible lid. (a) and (b) at 1500 °C, (c) the EDS analysis result of the highlighted point.

wires thicker (Fig. 10). It can be understood from Fig. 8a, due to the wide range of the synthesized wires and the thicker wires in the accumulated wires area center [30]. The thickness of this wires have been greater than 80 nm. Fig. 8c shows the EDS analysis of the flower-shaped B_4C synthesized by the carbon black precursor. The corresponding peaks to boron and carbon can be proved the synthesis of the boron carbide, and the cobalt peak can be related to the presence of the under catalyst the boron carbide belts. So that, the catalyst peak is presented in the EDS analysis and because the catalyst wasn't observed on the belt tip in the Fig. 8b, it can be concluded that the growth mechanism has been of the SLS type [4] and this nanobelts have been deviated from their growth route due to being subjected to the argon gas flow and have created a flower-shaped structure. One of the features of using carbon back as the precursor has been that the synthesis of a pigeonhole morphology is possible [6,31]. Thereby, the short belts are presented in the pigeonhole morphology and the morphology has changed to a flower-shaped which is shown in Fig. 8b.

Fig. 9a and b shows the SEM image of sample A at 1500 ^{o}C when the catalyst has been applied to the crucible lid. As can be seen, the argon gas

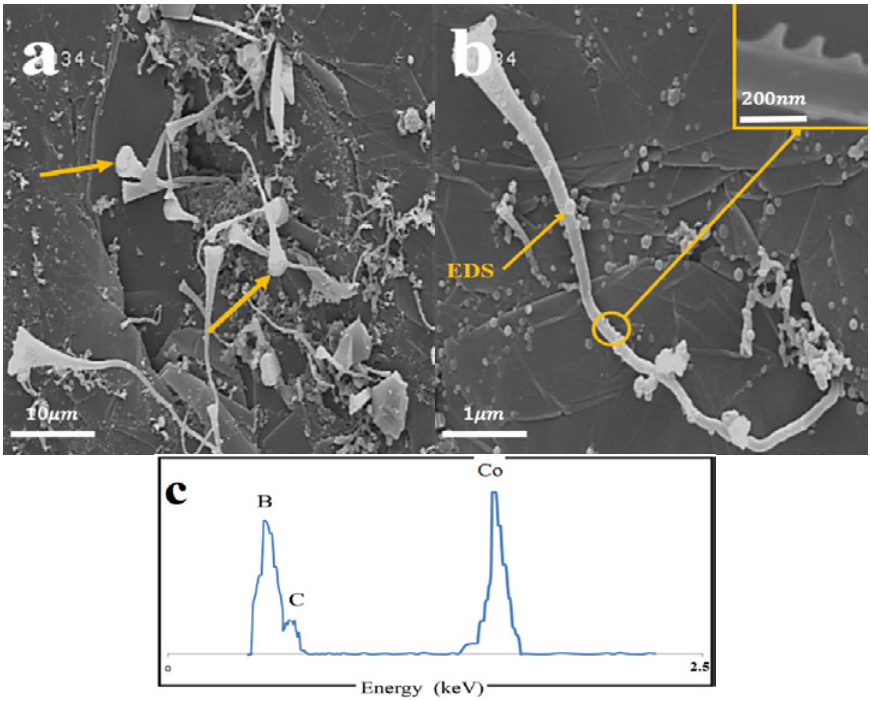

Fig. 9. the SEM image of the catalyst which has been applied to the crucible lid. (a) and (b) at 1500 ^{o}C with various magnifications, (c) the EDS analysis result of the highlighted point.

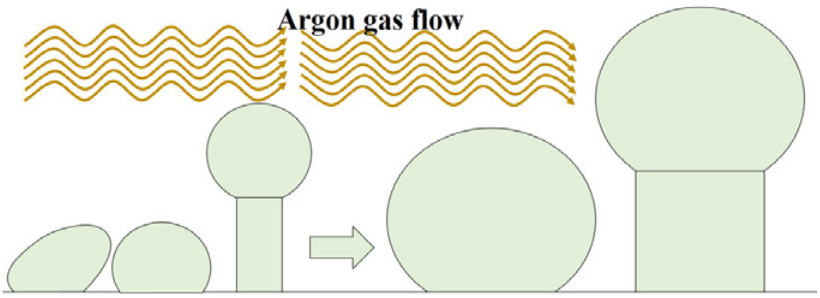

Fig. 10. The schematic of the joining catalyst droplets owing to the increased pressure of the crucible with increasing temperature and its effect on the diameter of the wires synthesized.

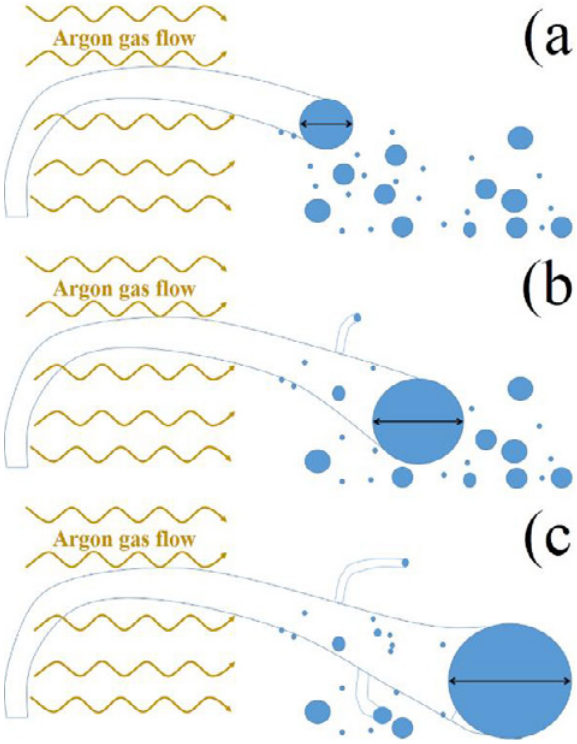

Fig. 11. The schematic of the effect of argon flow on the nanowires synthesized. (a) the argon flow resulted in the deviation of the wires, (b,c) the catalyst present at the wire tip combines with the catalyst droplets due to the deviation and grows.

flow has pulled the wires out of their path and are deviated to the flow direction. With this deviation, the catalyst at the tip of the wires are combined with other catalysts at the surface of the crucible lid and finally, the gradual coagulation of the present catalyst at the wire tip is occurred. Therefore, the synthesized nanowires thickness are gradually increased with the past time. With continuing this process, more the catalyst droplets was been added to the present catalyst at the wire tip and so that thicker wires are obtained. This process is caused to the needle-shaped nanowires can been synthesized. This nanowires are started at a thickness of about 100 nm and even less and are finished in a thickness of a few micrometers, this is shown schematically in Fig. 11. The interface between the catalyst and the nanowire falls into two classes, wetting or nonwetting [9]. Due to the tip of the wires in Fig. 9 a, the uneven interface of the liquid catalyst/ solid wires have indicated non-wetting of the catalyst [9]. The uneven interfaces are very important for nanostructures growth, because the atomic steps are easily generated at the bottom of such interfaces. In the uneven interfaces, there is often more than one low-energy liquid–solid interface during the growth of crystals and this is the source of uneven interfaces [32,33].

On the other hand, sticking the catalyst droplets present on the surface of the crucible lid was sticked to the surface of the synthesized nanowires and are leaded to the creation of new branches on the synthesized wires. Also, this new branches direction was changed to the direction of argon flow with the continuation of the process and finally, this process has formed the cactus-shaped morphology. If the argon flow is cut off and the VLS process continues, the bone-shaped morphology can been formed [32]. Fig. 9c shows the EDS analysis result of the highlighted point in Fig. 9b, the presence of the catalyst particles on tip of the boron carbide nanowires is proved the formation of sub-branches on the main branch.

CONCLUSION

In this research, B_4C nanowires are synthesized using carbon black as the precursor.

With increasing the temperature from 1500 ^oC to 1700 ^oC, nanowires and nanobelts are replaced with B_4C particles.

One of the advantages of using carbon black is

to synthesize nanoworms in a very little amount.

At 1500 °C, with decreasing the carbon particle size the synthesis efficiency of nanowires and nanobelts increases.

In general, increasing the synthesis temperature was favorable effected on the amount of the synthesized B_4C particle. Instead, this increasing the synthesis temperature has been formed the thicker nanowires and has been decreased the synthesis efficiency of nanowires.

The argon gas flow has formed the cactus-shaped nanowires by using activated carbon and the flower-shaped B_4C by using carbon black at 1500 °C.

Other morphologies of B_4C can been obtained by more delicate controlling the argon gas flow.

CONFLICT OF INTEREST

The authors declare that there are no conflicts of interest regarding the publication of this manuscript.

REFERENCES

1. Jung C-H, Lee M-J, Kim C-J. Preparation of carbon-free B_4C powder from B_2O_3 oxide by carbothermal reduction process. Mater Lett. 2004;58(5):609-614.
2. Anselmi-Tamburini U, Munir ZA, Kodera Y, Imai T, Ohyanagi M. Influence of Synthesis Temperature on the Defect Structure of Boron Carbide: Experimental and Modeling Studies. J Am Ceram Soc. 2005;88(6):1382-1387.
3. Anselmi-Tamburini U, Ohyanagi M, Munir ZA. Modeling Studies of the Effect of Twins on the X-ray Diffraction Patterns of Boron Carbide. Chem Mater. 2004;16(22):4347-4351.
4. Jazirehpour M, Alizadeh A. Synthesis of Boron Carbide Core−Shell Nanorods and a Qualitative Model To Explain Formation of Rough Shell Nanorods. The Journal of Physical Chemistry C. 2009;113(5):1657-1661.
5. Chen S, Wang DZ, Huang JY, Ren ZF. Synthesis and characterization of boron carbide nanoparticles. Appl Phys A. 2004;79(7):1757-1759.
6. Carlsson M, García-García FJ, Johnsson M. Synthesis and characterisation of boron carbide whiskers and thin elongated platelets. J Cryst Growth. 2002;236(1-3):466-476.
7. Lindström R, Maurice V, Zanna S, Klein L, Groult H, Perrigaud L, et al. Thin films of vanadium oxide grown on vanadium metal: oxidation conditions to produce V_2O_5 films for Li-intercalation applications and characterisation by XPS, AFM, RBS/NRA. Surf Interface Anal. 2005;38(1):6-18.
8. McIlroy DN, Zhang D, Kranov Y, Norton MG. Nanosprings. Appl Phys Lett. 2001;79(10):1540-1542.
9. McIlroy DN, Alkhateeb A, Zhang D, Aston DE, Marcy AC, Norton MG. Nanospring formation—unexpected catalyst mediated growth. J Phys: Condens Matter. 2004;16(12):R415-R440.
10. Welna DT, Bender JD, Wei X, Sneddon LG, Allcock HR. Preparation of Boron-Carbide/Carbon Nanofibers from a Poly(norbornenyldecaborane) Single-Source Precursor via Electrostatic Spinning. Adv Mater. 2005;17(7):859-862.
11. Jazirehpour M, Bahahrvandi H-R, Alizadeh A, Ehsani N. Facile synthesis of boron carbide elongated nanostructures via a simple in situ thermal evaporation process. Ceram Int. 2011;37(3):1055-1061.
12. Li-Hong B, Chen L, Yuan T, Ji-Fa T, Chao H, Xing-Jun W, et al. Synthesis and photoluminescence property of boron carbide nanowires. Chinese Physics B. 2008;17(12):4585-4591.
13. Johnsson M. Synthesis of boride, carbide, and carbonitride whiskers. Solid State Ionics. 2004;172(1-4):365-368.
14. Park B, Ryu Y, Yong K. GROWTH AND CHARACTERIZATION OF SILICON CARBIDE NANOWIRES. Surf Rev Lett. 2004;11(04n05):373-378.
15. Valcárcel V, Pérez A, Cyrklaff M, Guitián F. Novel Ribbon-Shaped α-Al_2O_3 Fibers. Adv Mater. 1998;10(16):1370-1373.
16. Liu H, Huang C, Teng X, Wang H. Effect of special microstructure on the mechanical properties of nanocomposite. Materials Science and Engineering: A. 2008;487(1-2):258-263.
17. Li YY, Cui JZ. The multi-scale computational method for the mechanics parameters of the materials with random distribution of multi-scale grains. Composites Sci Technol. 2005;65(9):1447-1458.
18. Liu HL, Huang CZ, Wang J, Liu BQ. Study on the Multi-Scale Nanocomposite Ceramic Tool Material. Key Eng Mater. 2006;315-316:118-122.
19. Kerti I, Toptan F. Microstructural variations in cast B4C-reinforced aluminium matrix composites (AMCs). Mater Lett. 2008;62(8-9):1215-1218.
20. Mohanty RM, Balasubramanian K, Seshadri SK. Boron carbide-reinforced alumnium 1100 matrix composites: Fabrication and properties. Materials Science and Engineering: A. 2008;498(1-2):42-52.
21. Oñoro J, Salvador MD, Cambronero LEG. High-temperature mechanical properties of aluminium alloys reinforced with boron carbide particles. Materials Science and Engineering: A. 2009;499(1-2):421-426.
22. Nhuapeng W, Thamjaree W, Kumfu S, Singjai P, Tunkasiri T. Fabrication and mechanical properties of silicon carbide nanowires/epoxy resin composites. Current Applied Physics. 2008;8(3-4):295-299.
23. Fiedler B, Gojny FH, Wichmann MHG, Nolte MCM, Schulte K. Fundamental aspects of nano-reinforced composites. Composites Sci Technol. 2006;66(16):3115-3125.
24. Wichmann MHG, Schulte K, Wagner HD. On nanocomposite toughness. Composites Sci Technol. 2008;68(1):329-331.
25. Vivekchand SRC, Ramamurty U, Rao CNR. Mechanical properties of inorganic nanowire reinforced polymer–matrix composites. Nanotechnology. 2006;17(11):S344-S350.
26. Thostenson E, Li C, Chou T. Nanocomposites in context. Composites Sci Technol. 2005;65(3-4):491-516.
27. Wagner RS, Ellis WC. VAPOR-LIQUID-SOLID MECHANISM OF SINGLE CRYSTAL GROWTH. Appl Phys Lett. 1964;4(5):89-90.
28. Morales AM, Lieber CM. A Laser Ablation Method for the Synthesis of Crystalline Semiconductor Nanowires. Science. 1998;279(5348):208-211.
29. Kolasinski K. Catalytic growth of nanowires: Vapor–liquid–solid, vapor–solid–solid, solution–liquid–solid and

solid–liquid–solid growth. Curr Opin Solid State Mater Sci. 2006;10(3-4):182-191.
30. Ma R, Bando Y. Investigation on the Growth of Boron Carbide Nanowires. Chem Mater. 2002;14(10):4403-4407.
31. Zhu YQ, Jin YZ, Kroto HW, Walton DRM. Co-catalysed VLS growth of novel ceramic nanostructuresElectronic supplementary information (ESI) available: TEM, SEM and HRTEM images for MgO, SiO_x and AlO_x ceramic nanomaterials. See http://www.rsc.org/suppdata/jm/b3/b312498n. J Mater Chem. 2004;14(4):685.
32. Lok SK, Wang G, Cai Y, Wang N, Zhong YC, Wong KS, et al. Growth temperature dependence of the structural and photoluminescence properties of MBE-grown ZnS nanowires. J Cryst Growth. 2009;311(9):2630-2634.
33. Wang N, Cai Y, Zhang RQ. Growth of nanowires. Materials Science and Engineering: R: Reports. 2008;60(1-6):1-51.